

Impact of High Concentrations of Saharan Dust Aerosols on Infrared-Based Land Surface Temperature Products

Francesco Stante , Sofia L. Ermida , Carlos C. DaCamara , Frank-Michael Göttsche , and Isabel F. Trigo 

Abstract—An analysis of three operational satellite-based thermal-infrared land surface temperature (LST) products is presented for conditions of heavy dust aerosol loading. The LST products are compared against ERA5’s skin temperature (SKT) across the Sahara Desert and Sahel region, where high concentrations of dust aerosols are prevalent. Large anomalous differences are found between satellite LST and ERA5’s SKT during the periods of highest dust activity, and satellite–ERA5 differences are shown to be strongly related to dust aerosol optical depth (DuAOD) at 550 nm, indicating an underestimation of LST in conditions of heavy dust aerosol loading. In situ measurements from two ground stations in the Sahel region provide additional evidence of this underestimation, showing increased biases of satellite LST with DuAOD, and no significant dependence of ERA5’s SKT biases on dust aerosol concentrations. The impact of atmospheric water vapor content on LST and SKT is also examined, but dust aerosols are shown to be the primary driver of the inaccurate LSTs observed. Based on comparisons with in situ data, we estimate an aerosol-induced underestimation of LST of approximately 0.9 K for every 0.1 increase in DuAOD. Analysis of brightness temperatures (BTs) in the thermal infrared atmospheric window reveals that dust aerosols have the opposite effect on BT differences compared to water vapor, leading to an underestimation of atmospheric correction by the LST retrieval algorithms. This article highlights a shortcoming of current operational LST retrieval algorithms that must be addressed.

Index Terms—Dust aerosols, land surface temperature (LST), Moderate Resolution Imaging Spectroradiometer (MODIS) LST, Spinning Enhanced Visible and InfraRed Imager (SEVIRI) LST.

I. INTRODUCTION

LAND surface temperature (LST) is an important variable of earth’s land surface, deeply involved in its energy balance, governing the processes of energy and water transfer at

the land–atmosphere interface. Satellite-based estimations of LST are the most efficient way to obtain extensive spatial and temporal coverage of this variable and are, therefore, highly valuable for local to global assessments of surface radiative and turbulent heat fluxes [1], [2], [3] and evapotranspiration [4], [5], [6]. Continuous records of LST enable a variety of more specific applications, such as the study of urban climates [7], [8], [9], the monitoring of agricultural droughts and vegetation health [10], [11], [12], [13], [14], or the characterization of wildfire intensities [15], [16].

Satellite-based LSTs are estimated most commonly from radiometric measurements in the thermal infrared (TIR) atmospheric window (8–13 μm). Estimating LST is a challenging task since multiple factors, such as surface properties, atmospheric composition, and satellite viewing geometry, affect the measured signal. These can be mostly accounted for via radiative transfer calculations, but require accurate knowledge of surface emissivity, vertical atmospheric profiles, and their respective effects on the measured TIR radiances. Numerous LST retrieval algorithms have been developed over the years [17] and many already provide LST with accuracies better than 1 K [18], [19], [20], [21], [22] under most surface and atmospheric conditions. However, despite continued development of these algorithms, they still have limitations and potential to be improved.

One limitation concerns retrievals under high aerosol loading. In the case of semiempirical methods, relating surface temperature with top-of-atmosphere brightness temperatures (BTs) in the TIR (split-window or mono-channel algorithms), a simplistic correction of aerosol effects is often included, assuming static average aerosol distributions during algorithm calibration [17], [23]. Although this approach is adequate for typical clear-sky conditions, the atmospheric transmissivity in the TIR decreases considerably in conditions of heavy aerosol loading [24] and this will lead to significant errors in LST retrievals if not properly accounted for. The impact of high aerosol concentrations on TIR-based retrievals of sea surface temperature (SST) has been studied since the 1980s [25], [26], [27], when stratospheric volcanic aerosols were found to cause a systematic underestimation of SSTs by up to 7 K following a major volcanic eruption. Motivated by strict accuracy requirements for global climate studies, SST retrievals have since addressed the effect of aerosols and today multiple aerosol-robust SST retrieval algorithms and

Manuscript received 30 December 2022; revised 28 February 2023; accepted 14 March 2023. Date of publication 31 March 2023; date of current version 2 May 2023. This work was supported by EUMETSAT and performed within the framework of the Satellite Applications Facility on Land Surface Analysis (<https://www.eumetsat.int/lisa-saf>). (Francesco Stante and Sofia L. Ermida are co-first authors.). (Corresponding author: Sofia L. Ermida.)

Francesco Stante, Sofia L. Ermida, and Isabel F. Trigo are with the Instituto Português do Mar e da Atmosfera, 1749-077 Lisbon, Portugal (e-mail: francesco.stante@ipma.pt; sofia.ermida@ipma.pt; isabel.trigo@ipma.pt).

Carlos C. DaCamara is with the Department of Geographic Engineering, Geophysics, and Energy and the Instituto Dom Luiz, Faculty of Sciences of the University of Lisbon, 1749-016 Lisbon, Portugal (e-mail: cdcamara@fc.ul.pt).

Frank-Michael Göttsche is with the Institute for Meteorology and Climate Research - Atmospheric Trace Gases and Remote Sensing, Karlsruhe Institute of Technology, 76131 Karlsruhe, Germany (e-mail: frank.goettsche@kit.edu).

Digital Object Identifier 10.1109/JSTARS.2023.3263374

aerosol-correction schemes exist [25], [26], [27], [28], [29], [30], [31], [32], [33], [34].

Despite the growing interest in developing aerosol-robust LST retrieval algorithms, operational LST products largely disregard this effect—either ignoring aerosols or simply flagging pixels with high aerosol concentrations. The articles published on this issue over the past decade [35], [36], [37], [38], [39], [40], [41] have generally focused on simulating the effect of aerosols on LST retrievals using radiative transfer models, showing a similar impact as on SST (i.e., an underestimation of LST with increased aerosol loading). In some studies, aerosol-robust algorithms [36], [38], [39] have already been proposed.

The aim of this article is to assess three operational and commonly used LST products in conditions of high dust aerosol concentrations, complementing the theoretical findings of previous modeling exercises [35], [36], [37], [39], [40], [41], as a first step toward building the case for the implementation of aerosol-robust algorithms in operational LST retrievals. We analyze the LST product provided by EUMETSAT’s Satellite Applications Facility on Land Surface Analysis (LSA SAF) [42] that uses a generalized split-window (GSW) algorithm applied to data from the Spinning Enhanced Visible and InfraRed Imager (SEVIRI) on board Meteosat Second Generation (MSG) satellites; and two LST products provided by NASA, both using data from the Moderate Resolution Imaging Spectroradiometer (MODIS) onboard the Terra and Aqua satellites—one employing a similar GSW algorithm [43] and the other a temperature-emissivity separation (TES) algorithm [44]. We focus here on the effect of dust aerosols as they are one of the most abundant types of aerosols by mass and have the highest maximum optical thickness of all aerosol types [45].

In the first part of this study (Section III-A), we compare the three LST products against the skin temperature (SKT) from ECMWF’s fifth-generation climate reanalysis, ERA5, over the Sahara Desert and surrounding regions—an area of high prevalence of dust aerosols [46], [47]. ERA5’s SKT corresponds to the temperature of the interface between the atmosphere’s lower model layer and the soil’s upper layer. It determines the long-wave radiation emitted by the model’s surface, being therefore physically equivalent to the satellite LST. It is well-known that ERA5’s SKT is not error (or bias-) free [48], [49], [50]. Indeed, ERA5’s SKT is not meant to be used here as an absolute reference for the LST products, but it is used instead as a spatially and temporally coherent dataset, appropriate to support consistency assessments of LST retrievals. The satellite–ERA5 differences (termed LST Delta) are assessed under varying atmospheric conditions, namely dust aerosol (Section III-B) and water vapor (Section III-C) concentrations, as represented by the Copernicus Atmosphere Monitoring Service (CAMS) global reanalysis of atmospheric composition, EAC4, and ERA5, respectively. The inherent differences between LST and SKT (more details in Section II-C) mean that the results from this analysis are only a first indication of the impact of dust aerosols on the examined LST products. The second part of this study (Sections III-D and III-E) makes use of in situ measurements from two ground stations within the domain of study to complement the results from the LST versus SKT comparisons. The stations are located

in the Sahel region (Niamey, Niger during 2006 and Dahra, Senegal from 2009 to 2013), south of the Sahara Desert, and provide in situ LSTs, which serve as an independent reference to both the satellite-based LST products and the reanalysis SKT. These stations are located in a region where high dust aerosol concentrations are frequent, making them particularly appropriate to assess LST retrievals under such conditions. To our knowledge, there are no previous studies providing a consistent comparison between satellite-retrieved LST (regardless of the algorithm) and in situ data under high aerosol loading. In the final part of this work (Section III-F), we examine MSG’s BTs used in the estimation of LST to show how dust aerosols affect the LST retrievals.

II. DATA AND METHODS

A. Area and Period of Study

This study is performed across the area delimited by latitude circles 40°N and 10°N, and by meridians 20°W and 40°E. This domain contains the Sahara Desert, which is an optimal location to analyze the effect of dust aerosols on LST retrievals: it is a vast region with a relatively homogenous surface, largely stable over time; it is the largest source of airborne dust particles on the globe [46], [47]; the atmosphere over the desert has a relatively low water vapor content [51], which means LST retrievals over this area are less affected by this critical atmospheric component; and it has negligible amounts of other types of aerosols (such as soot, organic matter, or sea-salt) [52]. We examine the effect of dust aerosols on LST retrievals during the year 2006 and the years 2009 to 2013, to ensure overlapping with the available in situ LSTs within the area of study.

B. Satellite Data

Three different satellite-based LST products are examined in this work, all derived from TIR top-of-atmosphere observations for clear-sky pixels. When comparing against ERA5’s SKT, all products are reprojected onto a regular grid of $0.25^\circ \times 0.25^\circ$. This reprojection is done by averaging all valid (i.e., cloud-free) LST datapoints inside each $0.25^\circ \times 0.25^\circ$ grid-box. During regridding, we exclude bundles with less than 70% valid pixels to minimize the impact of cloud contamination on our results. The comparison between satellite-based LST and in situ LST is performed using the original resolution of the satellite products. A brief description of the three LST products follows.

1) *MSG SEVIRI*: LSA SAF’s LST product [42] is based on radiance measurements of the SEVIRI sensor on-board MSG satellites and is retrieved with the GSW algorithm [53], [54]. It is available every 15 min in near-real-time in the original geostationary satellite projection (3 km at the subsatellite point) as well as on a regular $0.05^\circ \times 0.05^\circ$ grid. Here, we restrict our analysis to daytime observations between 8:00 UTC and 14:00 UTC, and to night-time observations between 20:00 UTC and 02:00 UTC, which ensures overlap with MODIS overpasses.

Special attention is given to this LST product in the last part of this work, where a more detailed analysis of the effect of dust aerosols on MSG observations is performed. Specifically,

TABLE I
DETAILS OF SATELLITE LST PRODUCTS ANALYZED

LST product	Platform	Sensor	Algorithm	Spatial Resolution	Temporal Resolution
LSA SAF's MSG/SEVIRI	MSG	SEVIRI	GSW	3 km (nadir)	15 min
NASA's MxD11	Terra and Aqua	MODIS	GSW	1 km	~12 hrs
NASA's MxD21	Terra and Aqua	MODIS	TES	1 km	~12 hrs

we examine the behavior of the BT difference between SEVIRI channels centered on 10.8 and 12.0 μm in relation to dust aerosol loading and water vapor. The BT data are also preprocessed to avoid cloud-contaminated values: first, its spatial resolution is adjusted to match ERA5's regular grid of $0.25^\circ \times 0.25^\circ$, during which all bundles with less than 70% cloud-free pixels are eliminated, taking into account the cloud mask of the MSG LST product. During this specific analysis, only desert pixels are considered, to reduce the impact of surface emissivity effects on the BT signal. Information on the landcover is obtained from the International Geosphere-Biosphere Program [55], which is currently used by LSA SAF to estimate MSG/SEVIRI emissivities [56], [57]. Datapoints with viewing zenith angle (VZA) above 42° are discarded to limit the effect of increased atmospheric path length on BT differences. This threshold is chosen as a compromise between having enough data for this analysis and limiting as much as possible the view-angle effects in atmospheric correction.

2) *Terra/Aqua MODIS*: The remaining two LST products are based on measurements of the MODIS sensor on-board Terra and Aqua, two satellites of NASA's Earth Observing System.

- a) MxD11 product: We consider the gridded MYD11C1 [58] and MOD11C1 [59] products for the comparisons against ERA5's SKT; and the Level-2 MYD11A1 [60] and MOD11A1 [61] products for the comparison against in situ data. The MxD11 product is derived using a GSW algorithm, similar to that of the LSA SAF SEVIRI product.
- b) MxD21 product: Following the strategy described above, we consider the gridded products MYD21C1 [62] and MOD21C1 [63] for comparisons against ERA5's SKT; and the Level-2 version, MYD21A1D [64], MYD21A1N [65], MOD21A1D [66], and MOD21A1N [67] for comparisons against in situ data ("D" and "N" indicate the day-time and night-time products, respectively). The MxD21 product is derived using a TES algorithm [68].

Terra and Aqua have sun-synchronous orbits (i.e., cross the equator at the same local time); for the study area, the day-time Terra overpass is between 8:00 UTC and 13:00 UTC; and between 20:00 UTC and 01:00 UTC for the night-time overpass, whereas that of Aqua is between 10:00 UTC and 14:00 UTC (between 22:00 UTC and 02:00 UTC) for the day-time (night-time) overpass. "C1" products have a spatial resolution of $0.05^\circ \times 0.05^\circ$ and "A1" products maintain the original 1 km resolution.

The details of the satellite LST products used are summarized in Table I.

C. ERA5 Data

ERA5 is the fifth-generation climate reanalysis from ECMWF [69]. The following three ERA5 variables are used throughout this study.

- 1) SKT, for the comparison against satellite LST.
- 2) Total cloud cover, to eliminate SKT data where cloud coverage is above 30%, following [48]. TIR-based LST products cover clear-sky conditions only and, therefore, meaningful satellite-model comparisons can only be performed considering (nearly) clear-sky SKT (e.g., [48], [50]).
- 3) Total column water vapor (TCWV), to assess the impact of atmospheric correction on the performance of LST algorithms, given that water vapor is the main component affecting the infrared bands used by the studied LST products.

All variables are provided in a $0.25^\circ \times 0.25^\circ$ grid with hourly temporal resolution.

ERA5's SKT represents the temperature at the interface between the model's soil and atmosphere, ensuring the closure of the surface energy balance. The SKT determines the model's surface thermal emission and, therefore, is physically compatible with LST estimates from TIR observations. SKT is not considered an absolute reference but, as shown in this work, is useful to diagnose the potential impact of dust aerosols on LST retrievals over an area with scarce in situ measurements. The conclusions drawn from the comparison between SKT and LST are later evaluated using in situ LST from two stations within the domain of study.

The satellite-based LST products are compared against SKT by computing their difference (as LST minus SKT), hereafter referred to as LST Delta, which is then systematically assessed for various ranges of dust aerosol and water vapor concentrations. For the calculation of LST Delta, ERA5's SKT values are directly matched to the hourly observations of SEVIRI/MSG and are linearly interpolated to the satellite observation time in the case of MODIS products.

D. CAMS Dust Aerosol Optical Depth (DuAOD) at 550 nm

Dust aerosol concentrations are obtained from EAC4, a CAMS global reanalysis optimized to estimate atmospheric composition [70]. EAC4 data are available three hourly on a $0.75^\circ \times 0.75^\circ$ grid. In this work, we use the DuAOD at 550 nm. CAMS DuAOD is only available for the visible range; however, since it is found to be linearly related to DuAOD in the TIR [71],

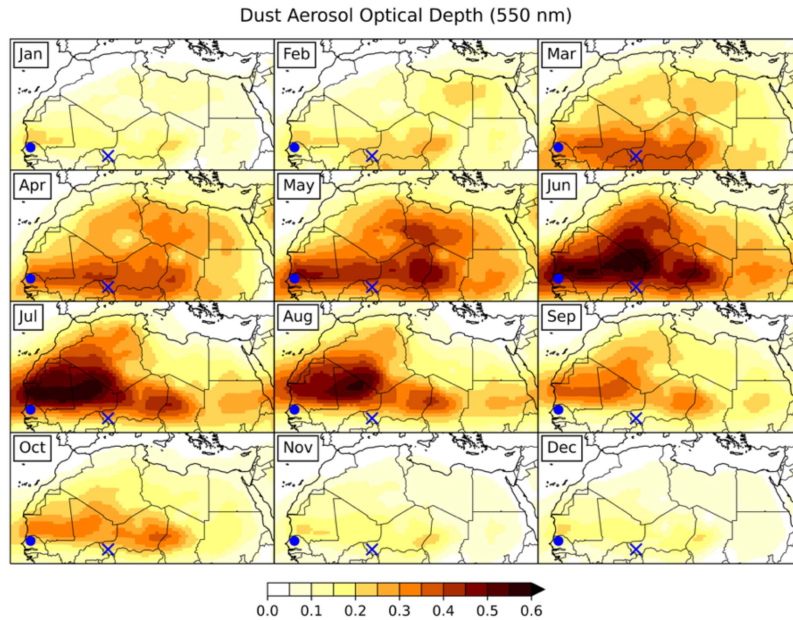


Fig. 1. Monthly averages of EAC4's DuAOD at 550 nm for years 2006 and 2009 to 2013. Values are unitless. The locations of the two stations that provide in situ LST are marked on the map: Niamey (cross) and Dahra (dot).

[72], [73], we consider it a suitable variable to quantify aerosol loading.

To analyze the relation between LST Delta and DuAOD, the DuAOD data are regridded with a nearest-neighbor approach to the $0.25^\circ \times 0.25^\circ$ grid adopted for all products and are linearly interpolated to match the respective LST retrieval times. Fig. 1 shows the monthly mean DuAOD corresponding to the observation times of MSG. Dust production and transport have a clear seasonality, with higher values in the south-western region of the Sahara Desert during June to August, in agreement with previous studies of dust aerosol distributions in this area [46], [47].

E. In Situ LST

In situ retrievals of LST are available from two locations within the area of study, obtained during two different periods. The first set of measurements was obtained by an Atmospheric Radiation Measurement mobile facility in Niamey, Niger, located at $13^\circ 28' 38.28''$ N, $2^\circ 10' 32.88''$ E (marked with a cross in Fig. 1), during 2006 [74]. This site provided downwelling and upwelling longwave radiation measured by broadband radiometers. The data are provided every minute, with data available from January 13, 2006 to December 8, 2006, from which LST can be calculated via Stefan–Boltzmann's law [75]

$$\text{LST} = \sqrt[4]{\frac{R_u - (1 - \varepsilon_{BB}) R_d}{\varepsilon_{BB} \sigma_{SB}}} \quad (1)$$

where R_u and R_d are the measured upward and downward longwave radiances, respectively, ε_{BB} is the surface broadband emissivity, and σ_{SB} is the Stefan–Boltzmann constant. Broadband emissivity of the site is obtained from the ASTER Global Emissivity Dataset 100-m V003 [76].

The second set of in situ LST originates from an LST validation station operated by the Karlsruhe Institute of Technology in Dahra, Senegal, located at $15^\circ 24' 8.28''$ N, $15^\circ 25' 58.08''$ W (marked with a dot in Fig. 1), from 2009 to 2013 [77]. The station is equipped with narrow-band radiometers measuring surface upwelling and atmospheric downwelling radiances from wavelengths of 9.6 to $11.5 \mu\text{m}$. The data are provided every minute, in the period between July 12, 2009 and December 31, 2013. The LST is calculated by inverting Planck's function

$$B_\lambda(\text{LST}) = \frac{L_{\lambda,u} - (1 - \varepsilon_\lambda) L_{\lambda,d}}{\varepsilon_\lambda} \quad (2)$$

where λ is the radiometer central wavelength ($10.55 \mu\text{m}$), $L_{\lambda,u}$ and $L_{\lambda,d}$ are the upwelling and downwelling radiance measured by the station radiometers, and ε_λ is the surface emissivity at λ . In this case, the emissivity estimates are those derived for the SEVIRI/MSG channel centered on $10.8 \mu\text{m}$, which is close to the radiometers' central wavelength (following [77]).

These two sets of in situ LST are used as an independent reference for the satellite-based LSTs and ERA5's SKT. Further precautions are taken to avoid selecting cloud-contaminated data, especially during the wet season, when the Intertropical Convergence Zone (ITCZ) crosses the stations [78], [79]. First, only satellite datapoints where all surrounding pixels are cloud-free are used: if only one of the eight surrounding pixels is cloud-contaminated, the satellite datapoint is discarded. Second, only SKT datapoints where the corresponding MSG LST is cloud-free (according to the previous condition) are used, to avoid comparing cloudy in situ observations against clear-sky ERA5 data. Furthermore, the in situ observations are averaged over 5-min intervals centered at the satellite/reanalysis observation/simulation time, in order to minimize the effect of fluctuations in the ground observations.

Similar to the analysis of LST Delta, the differences between satellite-LST/ERA5-SKT and in situ LST (as satellite-LST/ERA5-SKT minus in situ LST), termed LST Error, are calculated and systematically compared to DuAOD and water vapor content. Additionally, the bias, the dispersion, and the uncertainty of each satellite-LST/ERA5-SKT product with respect to the in situ LSTs are calculated. These calculations follow the recommendations by the Committee on Earth Observation Satellites Working Group on Calibration and Validation – Land Product Validation Subgroup. Accordingly, the robust bias between satellite-LST/ERA5-SKT and in situ LST is given by the median error

$$\mu = \text{median}(LST_{sat/rea} - LST_{insitu}) \quad (3)$$

where $LST_{sat/rea}$ and LST_{insitu} represent the satellite-LST/ERA5-SKT and in situ LST, respectively. The dispersion of the differences between satellite-LST/ERA5-SKT and in situ LST is given by the robust standard deviation (SD)

$$\sigma = \text{median}(|(LST_{sat/rea} - LST_{insitu}) - \mu|) \times 1.4826. \quad (4)$$

The root-mean-square error (RMSE) of the satellite/reanalysis products is computed as

$$\text{RMSE} = \sqrt{\frac{(LST_{sat/rea} - LST_{insitu})^2}{N}} \quad (5)$$

where N is the sample size.

III. RESULTS

A. Comparison of Satellite LST Against ERA5's SKT

Monthly averages of LST Delta for the area and period of study are presented in Fig. 2 for the three investigated LST products (MSG, MxD11, and MxD21). In agreement with previous studies [48], [49], [50], [80], [81], ERA5's SKT has an overall cold bias with respect to satellite-based LST (i.e., LST Delta is positive), throughout most months over most of the area. However, strong negative LST Delta values can be observed in all three comparisons during summer (June, July, and August), when concentrations of dust aerosols are generally higher (see Fig. 1). These results suggest that high concentrations of dust aerosols might be affecting LST retrievals, leading to an underestimation of LST and the observed negative values of LST Delta.

Negative LST Delta are particularly pronounced in the MODIS products, which have lower values than the MSG product. The variable viewing geometry of MODIS (and longer optical paths) increases the sensitivity of the product to aerosols and may at least partially explain the differences between MODIS and MSG when compared against ERA5. Differences are also observed between the MODIS products: MxD21 shows a more localized negative pattern than MxD11, particularly at the southern edge of the domain. However, during summer months (wet season) the atmospheric water vapor content in this region is particularly high due to the position of the ITCZ [78], [79], which is also associated with a strong greening of the vegetation. As such, the discrepancy seen between LST products in this area

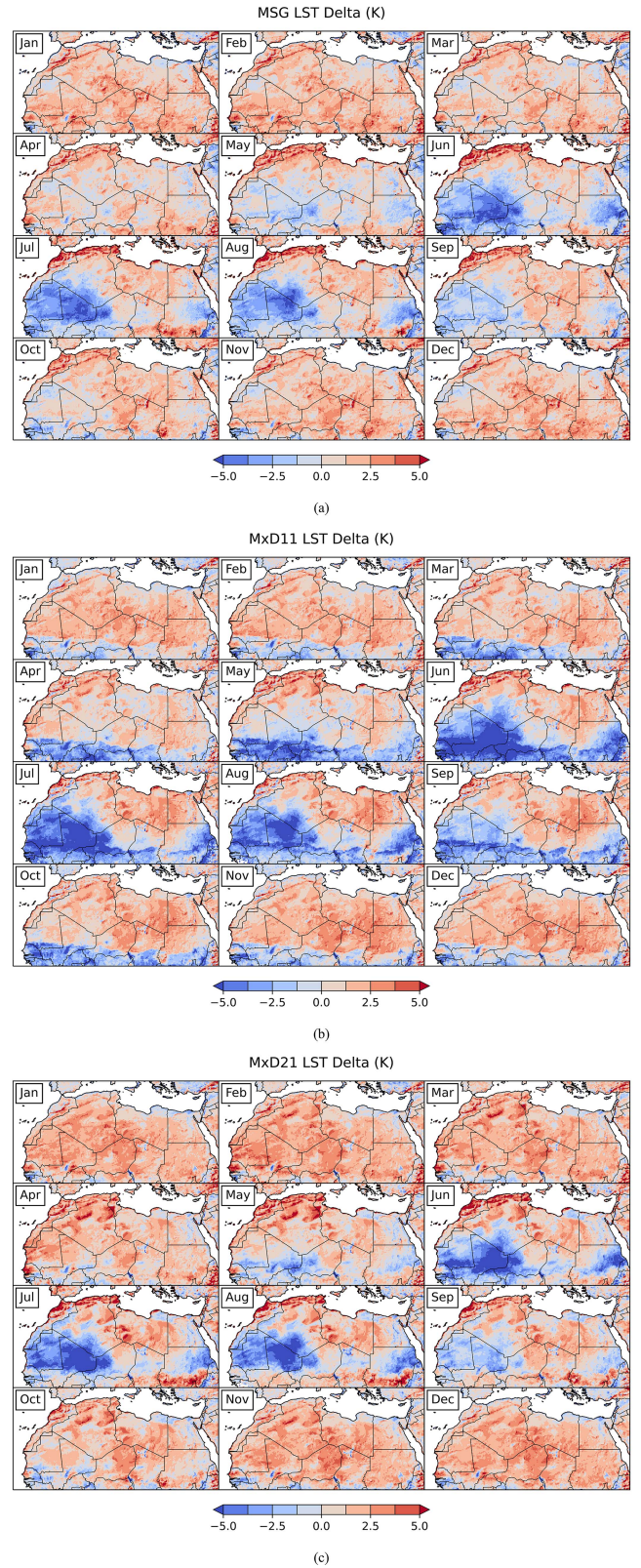


Fig. 2. Monthly averages of LST Delta (daytime and night-time combined) for years 2006 and 2009 to 2013, for each LST product: (a) MSG; (b) MxD11; and (c) MxD21.

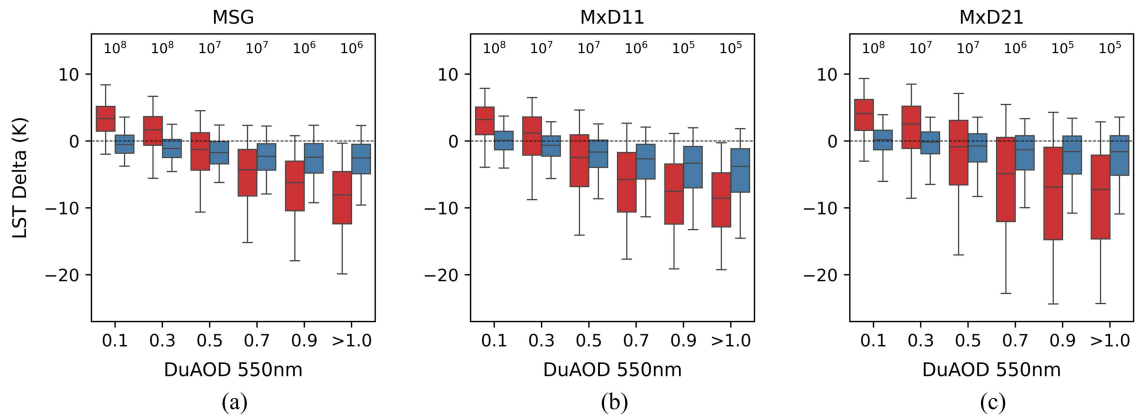


Fig. 3. Boxplots of LST Delta for six classes of DuAOD for each LST product: (a) MSG; (b) MxD11; and (c) MxD21. Red boxes correspond to daytime and blue boxes to night-time observations. The black horizontal lines in the boxes indicate the median, the box limits the 25th and 75th percentiles, and the whiskers the 5th and 95th percentiles. The x -axis labels indicate the center points of each DuAOD class, except for the last class where the lower bound is indicated. The number above each pair of boxes indicates the number of datapoints used in each class, which was similar for daytime and night-time observations.

could be related to differences in atmospheric correction and/or surface emissivity estimates.

To better examine the role of dust aerosol and water vapor concentrations on values of LST Delta, a statistical analysis of the relation between LST Delta and these two variables follows.

B. Relation Between LST Delta and DuAOD

To assess the relation between LST Delta and dust aerosol loading, the DuAOD data are subdivided into six classes: $\text{DuAOD} \leq 0.2$, $0.2 < \text{DuAOD} \leq 0.4$, $0.4 < \text{DuAOD} \leq 0.6$, $0.6 < \text{DuAOD} \leq 0.8$, $0.8 < \text{DuAOD} \leq 1.0$, and $\text{DuAOD} > 1.0$. The LST Delta values for each LST product are then sorted into the respective DuAOD class. The resulting LST Delta distributions are shown in Fig. 3 for daytime (red) and night-time (blue) separately.

Under low dust aerosol loading ($\text{DuAOD} \leq 0.4$) LST Delta values are predominantly positive for daytime observations, independently of the LST product considered, and slightly negative for night-time observations. This is in agreement with the patterns seen in Fig. 2 for regions with low dust aerosol concentrations. More significantly, and as expected from the results of the previous section, LST Delta values of each LST product decrease with increasing dust aerosol concentration, independent of the time of day, although the sensitivity to DuAOD seems to be stronger for daytime observations. In all LST products, there is a noticeable increase in the interquartile range for higher DuAOD classes. This could be partially related to increased DuAOD variability in situations of high aerosol concentrations that may not be well captured by the coarse temporal and spatial resolution of the CAMS reanalysis.

C. Relation Between LST Delta and TCWV

The relation between water vapor and LST Delta is examined in analogy to the dust aerosol loading. The TCWV data are subdivided into the following six classes: $\text{TCWV} \leq 10$, $10 < \text{TCWV} \leq 20$, $20 < \text{TCWV} \leq 30$, $30 < \text{TCWV} \leq 40$, $40 < \text{TCWV} \leq 50$, $\text{TCWV} > 50$ (kg/m^2). The LST Delta distributions for each LST product and TCWV class

are shown in Fig. 4, separated into daytime (red) and night-time (blue) observations.

LST Delta shows a significantly lower dependence on TCWV than for DuAOD (see Fig. 3), although all LST products tend to have positive LST Delta values for drier atmospheres and negative or lower LST Delta values for moister atmospheres. However, while Fig. 3 revealed a systematic change in LST Delta with DuAOD, regardless of the satellite sensor or LST algorithm, the variation of LST Delta with TCWV is less pronounced and appears to be dependent on the respective algorithms' atmospheric correction.

D. Comparison of Satellite LST Against In Situ LST – Niamey

For an independent assessment of the three LST products (and ERA5's SKT), we now compare these products against in situ LST, starting with the data from the Niamey site. Fig. 5 displays the satellite LST and ERA5's SKT datapoints versus the corresponding in situ LST for northern hemisphere winter (DJF) and summer (JJA) months, the seasons with the lowest and highest dust aerosol concentrations, respectively. The corresponding bias, dispersion, and RMSE of the satellite LST and reanalysis SKT products are presented in Table II.

MSG LSTs are in general agreement with ground measurements during winter months, showing a bias of -1.46 K (0.73 K) for the daytime (night-time) and relatively low SD and RMSE, with values of 1.17 K (1.05 K) and 2.35 K (1.34 K) for the daytime (night-time) observations, respectively. The MODIS products show overall higher dispersion and a stronger contrast between daytime and night-time overpasses. MxD11 presents a strong negative daytime bias (-4.48 K), which is significantly reduced to -0.85 K for night-time overpasses; the SD and RMSE also decrease significantly between day and night, from 3.72 to 1.41 K and from 6.18 to 2.67 K, respectively. In contrast, MxD21 has a weaker daytime bias (-0.38 K) compared to night-time (2.32 K), whereas the dispersion (SD) and RMSE also decrease from daytime to night-time (from 2.91 to 1.45 K and from 5.11 to 2.83 K, respectively). The higher dispersion of the MODIS products compared to MSG seems to be related to the variability

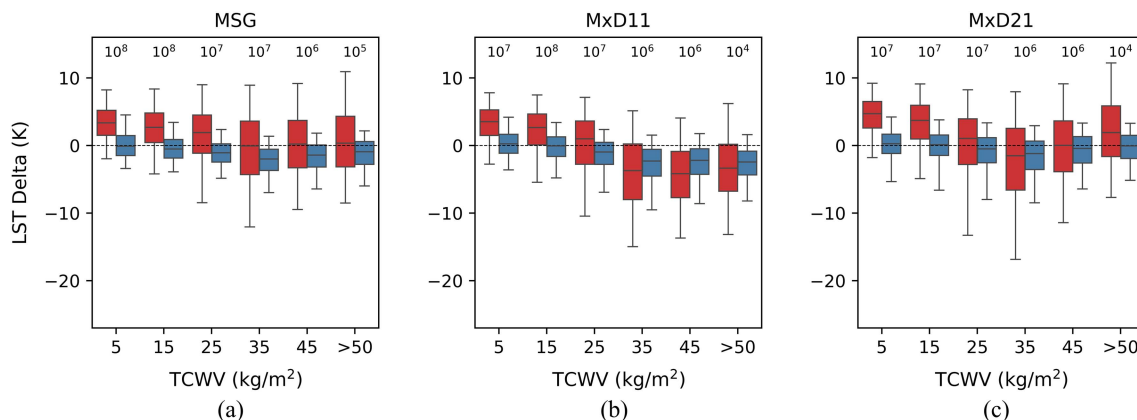


Fig. 4. As Fig. 3, but for the relation between LST Delta and TCWV.

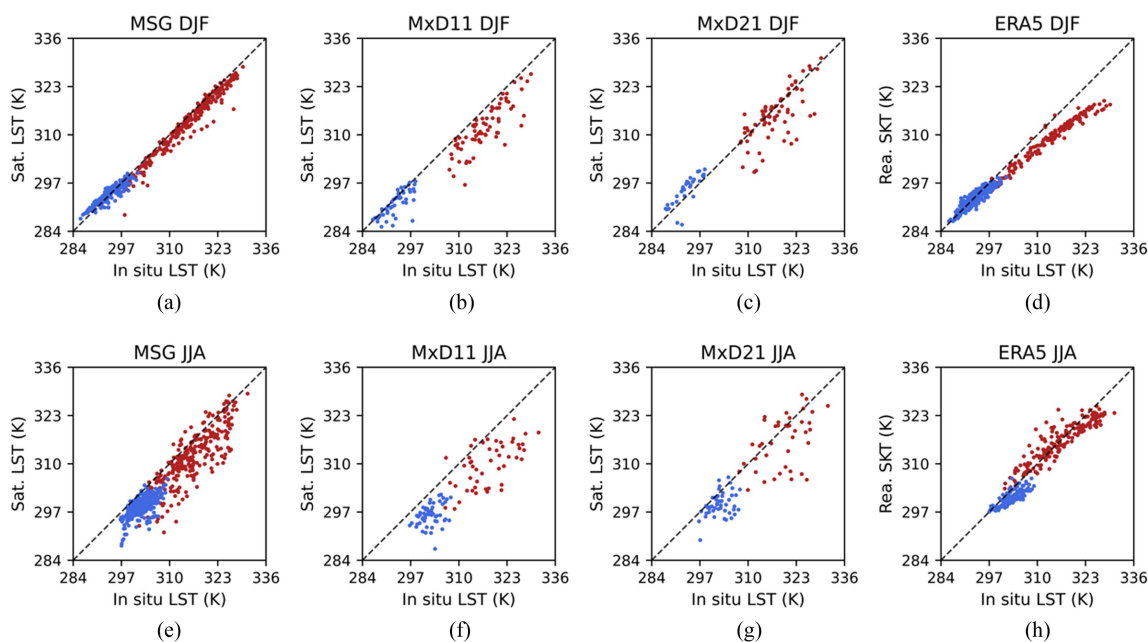


Fig. 5. Comparison of satellite LST and ERA5’s SKT against in situ LST at Niamey during winter months (top panels) and summer months (bottom panels) for 2006. Red dots correspond to daytime observations and blue dots to night-time observations.

TABLE II

STATISTICS OF THE COMPARISON BETWEEN SATELLITE LST AND ERA5’S SKT AGAINST IN SITU LSTS AT NIAMEY: MEAN DIFFERENCE (μ) IN K, SD OF THE DIFFERENCE (σ) IN K, RMSE IN K, AND THE NUMBER OF DATAPPOINTS (N)

LST Product	MSG		MxD11		MxD21		ERA5	
	DJF	JJA	DJF	JJA	DJF	JJA	DJF	JJA
Daytime								
μ	-1.46	-3.70	-4.48	-8.64	-0.38	-2.62	-4.50	-0.37
σ	1.17	3.78	3.72	5.75	2.91	6.50	2.19	3.09
RMSE	2.35	5.95	6.18	9.70	5.11	7.43	6.63	3.10
N	244	263	71	49	71	41	165	171
Night-time								
μ	0.73	-3.41	-0.85	-5.09	2.32	-2.55	-0.38	-2.12
σ	1.05	1.96	1.41	2.53	1.45	3.13	1.56	1.43
RMSE	1.34	4.47	2.67	6.86	2.83	4.68	1.49	2.62
N	237	264	49	55	32	48	194	124

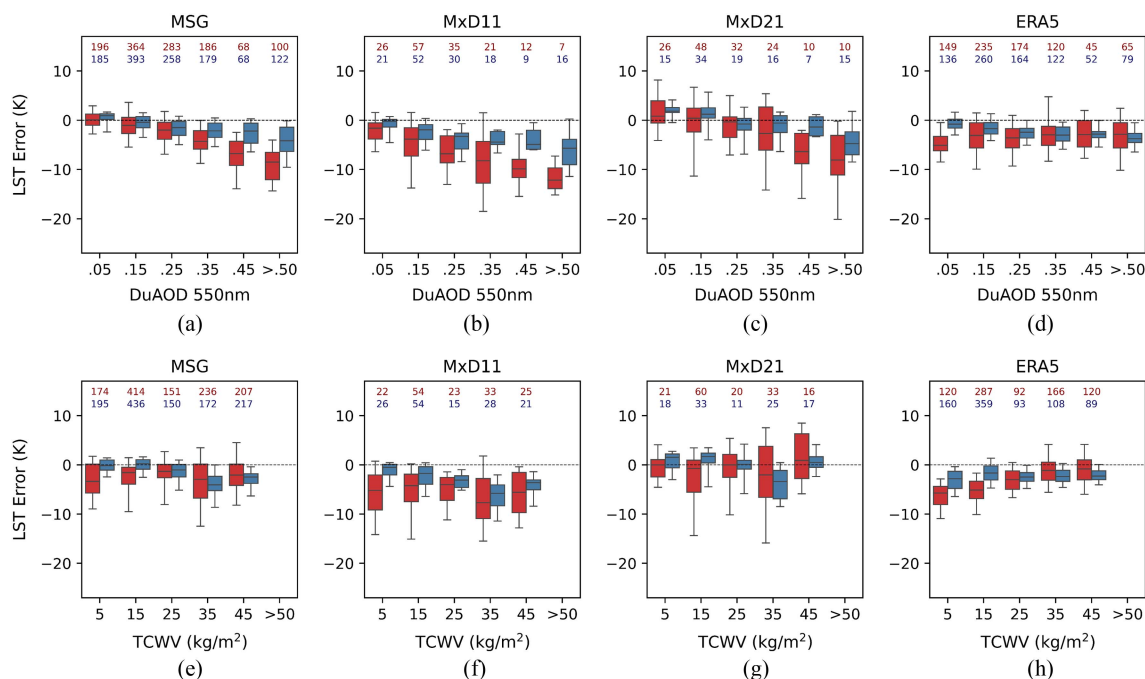


Fig. 6. Boxplots of LST Error for six classes of DuAOD (top panels) and of TCWV (bottom panels) at Niamey in 2006, comparing in situ LST to: (a) and (e) MSG LST; (b) and (f) MxD11 LST; (c) and (g) MxD21 LST; (d) and (h) ERA5's SKT. Red boxes correspond to daytime and blue boxes to night-time observations. The black horizontal lines in the boxes indicate the median, the box limits the 25th and 75th percentiles, and the whiskers the 5th and 95th percentiles. The x-axis labels indicate the center points of each DuAOD class, except for the last class where the lower bound is indicated. The number above each box represents the number of datapoints used in each distribution, color-coded for time of day.

in the viewing geometry of satellites with polar orbit. In fact, we found that LST Deltas for high DuAOD tend to increase with increasing view angle (not shown). Finally, ERA5's SKT presents a significant daytime cold bias of -4.50 K (with SD of 2.19 K). Its RMSE (6.63 K) is high due to the high bias value. At night, the bias (-0.38 K), dispersion (1.56 K), and RMSE (1.49 K) are all lower. These results are in agreement with previous works showing that ECMWF SKT tends to underestimate the daily amplitude in arid and semiarid conditions (e.g., [48], [49], [50]).

In summer months, a period of higher prevalence of dust aerosols in Niamey (see Fig. 1), all satellite LST products present stronger negative biases, larger dispersions, and higher uncertainties. The daytime (night-time) biases increase to -3.70 K (-3.41 K), -8.64 K (-5.09 K), and -2.62 K (-2.55 K) for MSG, MxD11, and MxD21 products, respectively, and the corresponding RMSE increases to 5.95 K (4.47 K), 9.70 K (6.86 K), and 7.43 K (4.68 K). This indicates less accurate LST retrievals during this season and is consistent with the previous conclusions that heavy dust aerosol loading causes LST to be underestimated. Interestingly, ERA5's daytime cold bias is significantly reduced to -0.37 K but increased (-2.12 K) for night-time simulations. The reasons for this seasonal change in ERA5 accuracy are out of scope of this work: these may be related to effects of aerosols on radiation fluxes, changes in surface fluxes and their simulation during the wet season (as opposed to those in the dry DJF season), or even due to compensation by other errors. Nevertheless, this result confirms that the comparisons between SKT and LST must be taken with caution.

To assess the role of dust aerosol and water vapor concentrations on the LST Errors (i.e., satellite LST or ERA5's SKT minus in situ LST), a similar statistical analysis as presented in Sections III-B and III-C is performed. For this analysis, the data for the entire year 2006 are used. Fig. 6 displays the relationship between LST Error and DuAOD (top panels) and TCWV (bottom panels), separated into daytime (red) and night-time (blue) observations. The panels clearly show an increased underestimation of all satellite LST products with increased DuAOD. For these products, the relation between the LST Error and TCWV is less steady, but all exhibiting a local minimum for TCWV values between 30 and 40 kg/m^2 . The limited sample size should be noted, especially in the case of MODIS products. Regarding ERA5's SKT, the LST Error shows a small dependence on DuAOD and a slightly stronger dependence on TCWV. Daytime cool biases tend to be larger for dry atmospheres and low DuAOD (more frequent during the dry season), being likely that multiple factors, such as seasonal variation in soil moisture, the representation of vegetation cover and radiative fluxes at the surface, and their respective role on the sensible/latent heat partition, play a role here [49].

E. Comparison of Satellite LST Against In Situ LST – Dahra

We now examine the satellite LST products over the Dahra site during the years 2009–2013. Fig. 7 displays the comparisons of satellite LST (and ERA5's SKT) against in situ LST. Table III presents the corresponding statistical results.

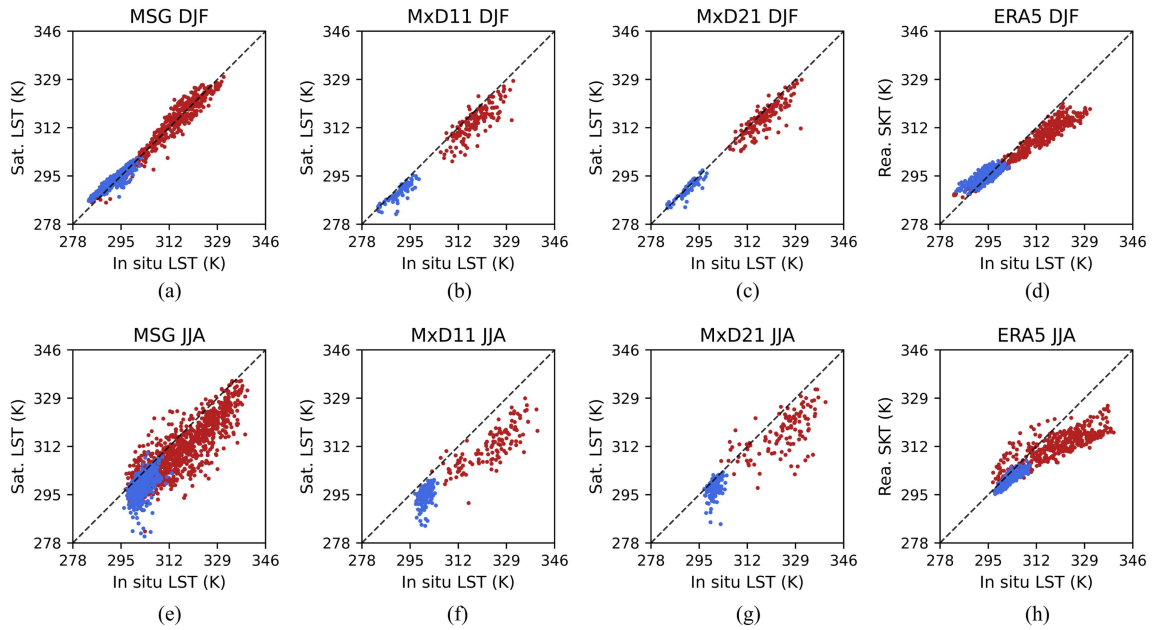


Fig. 7. Comparison of satellite LST and ERA5's SKT against in situ LST at Dahra during winter months (top panels) and summer months (bottom panels) for 2009–2013. Red dots correspond to daytime observations and blue dots to night-time observations.

TABLE III

STATISTICS OF THE COMPARISON BETWEEN SATELLITE LST AND ERA5'S SKT AGAINST IN SITU LSTs AT DAHRA: MEAN DIFFERENCE (μ) IN K, SD OF THE DIFFERENCE (σ) IN K, RMSE IN K, AND THE NUMBER OF DATAPOINTS (N)

LST Product	MSG		MxD11		MxD21		ERA5	
	DJF	JJA	DJF	JJA	DJF	JJA	DJF	JJA
Daytime								
μ	-0.09	-5.09	-3.57	-11.16	-1.75	-6.87	-3.67	-5.99
σ	1.97	4.51	3.19	4.32	1.97	5.71	3.48	7.01
RMSE	2.30	7.54	5.07	12.32	3.85	10.35	5.49	9.32
N	517	1140	154	133	156	115	406	521
Night-time								
μ	0.57	-3.06	-2.01	-4.87	-0.50	-2.86	0.48	-2.12
σ	1.08	2.29	1.34	2.18	1.39	2.52	2.32	1.06
RMSE	1.52	4.51	2.79	6.29	1.66	4.31	2.41	2.39
N	470	1081	81	153	64	135	376	576

Overall, the results for Dahra are well aligned with those for Niamey. During winter months MSG LST is in good agreement with station LST, with a bias of only -0.09 K during the day and 0.57 K at night, and relatively low SD (1.97 K at daytime and 1.08 K at night-time) and RMSE (2.30 K at daytime and 1.52 K at night-time). For DJF, MODIS products show reduced dispersion compared to Niamey and smaller contrast between day and night-time. MxD21 performs better than MxD11 at any time of day, with smaller biases, SD (except during night-time, where both values are similar), and RMSE. For daytime, ERA5's SKT shows a cold bias of -3.67 K in DJF (SD of 3.48 K) and high RMSE of 5.49 K. As for Niamey, the night-time bias (0.48 K), the dispersion (2.32 K), and the uncertainty (2.41 K) are all lower.

Just as in Niamey, all satellite LST products show stronger negative biases for JJA, as well as larger dispersion and higher uncertainties than for the winter months, for both daytime and

night-time observations. The daytime (night-time) biases increase to -5.09 K (-3.06 K), -11.16 K (-4.87 K), and -6.87 K (-2.86 K) for the MSG, MxD11, and MxD21 products, respectively, whereas RMSE increases to 7.54 K (4.51 K), 12.32 K (6.29 K), and 10.35 K (4.31 K). Regarding ERA5's SKT, we see an increase in its night-time bias (to -2.12 K), as well as in the daytime value (to -5.99 K), in contrast to Niamey, where ERA5 daytime statistics are better for JJA. However, while the SD and RMSE increase during daytime (to 7.01 and 9.32 K, respectively), they decrease during night-time (to 1.06 and 2.39 K). Again, these results, together with the ones for Niamey, show the limitations of using ERA5's SKT as an absolute diagnostic reference for LST and highlight the need for independent ground measurements.

As in the previous section, the relation between LST Error and dust aerosol and water vapor concentrations is analyzed

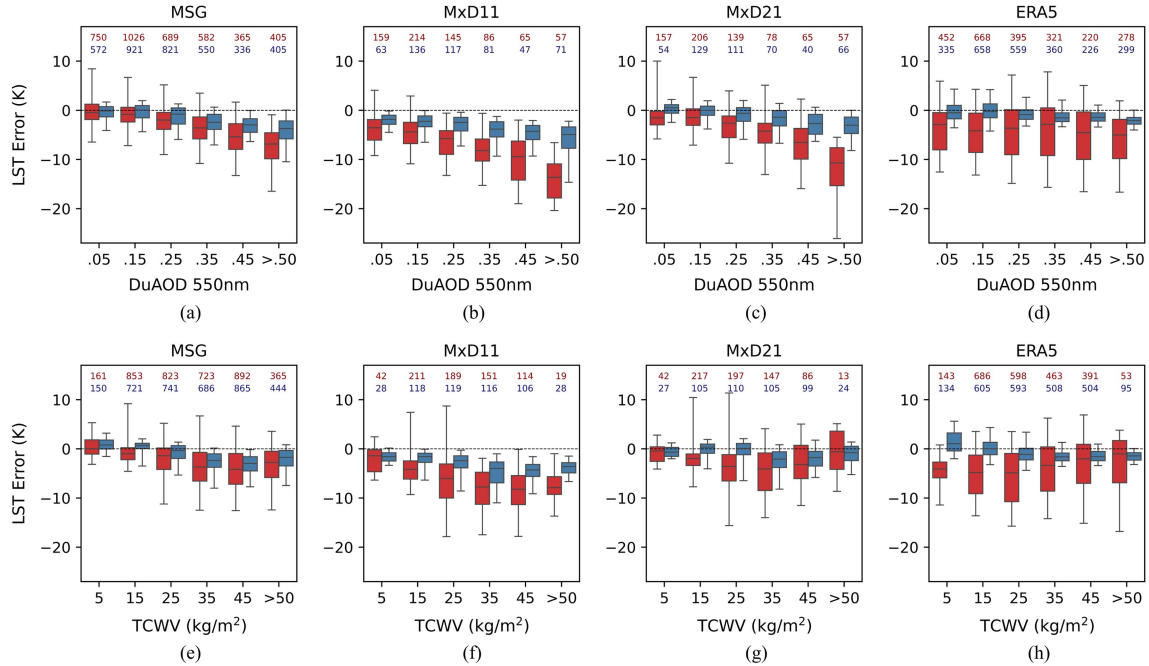


Fig. 8. Boxplots of LST Error for six classes of DuAOD (top panels) and of TCWV (bottom panels) at Dagra during 2009–2013, comparing in situ LST to: (a) and (e) MSG LST; (b) and (f) MxD11 LST; (c) and (g) MxD21 LST; (d) and (h) ERA5’s SKT. Red boxes correspond to daytime and blue boxes to night-time observations. The black horizontal lines in the boxes indicate the median, the box limits the 25th and 75th percentiles, and the whiskers the 5th and 95th percentiles. The x-axis labels indicate the center points of each DuAOD class, except for the last class where the lower bound is indicated. The number above each box represents the number of datapoints used in each distribution, color-coded for time of day.

statistically (see Fig. 8) for the entire years 2009–2013. The panels show similar results to the ones for Niamey, i.e., an increased underestimation of all LST products with increased dust aerosol loading. The relation with TCWV is similar for all satellite LST products, with the largest median LST Error around the fourth and fifth TCWV class. ERA5’s LST Error exhibits no obvious dependence on DuAOD and a noticeable dependence on TCWV (especially at daytime), similar to Niamey.

F. MSG BT Analysis

To better understand the underestimation of satellite-based LSTs under heavy aerosol loading, we perform a more detailed analysis of MSG data. In particular, we analyze the BT difference between the channels centered on 10.8 and 12.0 μm, as it is explicitly used in the GSW algorithm and implicitly impacts the TES approach. Here, we only analyze BT differences (and not the BT mean) since BT values vary strongly with the season, making it difficult to decouple the effects of aerosol loading, atmospheric water vapor, and LST amplitude. The BT difference is predominantly determined by the emissivity of the surface and the transmissivity of the atmosphere. It is therefore useful to study how the BT difference varies with dust aerosol concentrations as this might help understand the underestimation of LST.

Fig. 9 shows the two-way dependence of BT differences on DuAOD and TCWV for the desert region of the study area where $VZA < 42^\circ$, for the entire period of study. The data clearly show that BT differences increase with TCWV (underlining

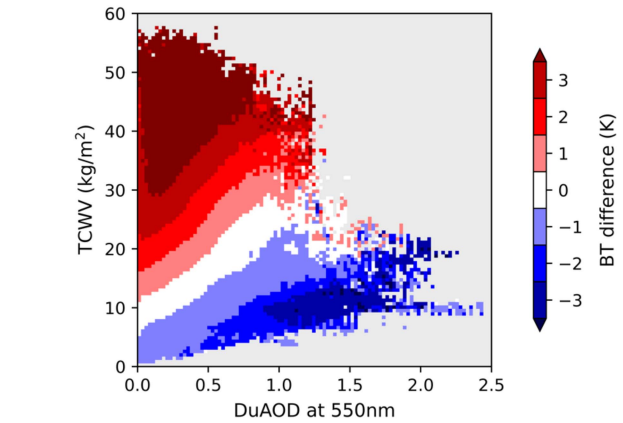


Fig. 9. BT difference ($BT_{10.8} - BT_{12.0}$) as a function of DuAOD and TCWV. Only contains datapoints where $VZA < 42^\circ$ and landcover is desert.

the role of water vapor in the GSW algorithm) and decrease with DuAOD. When water vapor and dust aerosol concentrations are low, typical of winter months, BT differences are negative since desert emissivities at 12.0 μm are generally higher than at 10.8 μm. In summer months, when water vapor and dust aerosol concentrations are higher, the BT difference may be negative or positive, and for certain combinations of water vapor and dust aerosol concentrations, their effect can balance out.

The increased BT difference with TCWV is a well-studied behavior [17]: water vapor mainly affects the “dirty” 12.0 μm

channel, significantly decreasing the transmissivity of the atmosphere in this channel compared to the $10.8 \mu\text{m}$ channel and resulting in an increasingly positive BT difference with increased water vapor. The behavior of BT difference with DuAOD is consistent with the optical properties of dust aerosols: the imaginary part of the complex index of refraction of dust aerosols is higher in the $10.8 \mu\text{m}$ channel than in the $12.0 \mu\text{m}$ channel [82], [83], meaning that an atmosphere with heavy dust aerosol loading will have a lower transmissivity in the $10.8 \mu\text{m}$ channel, resulting in a progressively lower BT difference with increased dust aerosol concentrations. This result is also in agreement with findings from previous studies of the aerosol effect in the TIR [29], [32], [35], [41].

These changes in transmissivity due to dust aerosols, combined with the additional atmospheric emission caused by them, will introduce large errors in LST retrievals for two reasons: 1) by affecting the mean BT, which is also an essential component of the GSW algorithm; 2) by changing the expected dependence of the BT differences on TCWV, which is critical in algorithms such as the GSW. In the case of the TES, the emissivity retrieval is based on the spectral contrasts between the different channels. Therefore, any contribution of the atmosphere to the observed BT spectral contrasts not accounted for may introduce significant errors to the emissivities [20].

IV. DISCUSSION

Satellite-based estimations of LST are a valuable asset in the global study of earth's land surface. However, current TIR LST products largely ignore the effect of aerosols on satellite retrievals, either by only using simplistic approaches (e.g., using average aerosol loadings or profiles in the simulations for algorithm calibration) or by not accounting for this effect at all [43], [84], [85], [86], [87]. In this work, we evaluate the performance of three operational LST products (LSA SAF's SEVIRI/MSG and NASA's MxD11 and MxD21) in conditions of heavy dust aerosol loading, assessing them over the Sahara Desert and the Sahel region, where high concentrations of dust aerosols frequently occur. The LST products are compared against ERA5's SKT over this domain, as well as against in situ measurements from two ground stations within it. We provide compelling evidence that current LST products underestimate in conditions of heavy dust aerosol loading, complementing previous findings from modeling exercises about the impact of aerosols on LST retrievals [35], [36], [37], [38], [39], [40], [41].

A. Comparison of Satellite LST Against ERA5's SKT

In order to understand the spatial and temporal extent of aerosol-affected LST retrievals, we compare the three LST products against a corresponding reanalysis variable, ERA5's SKT. Several works indicate that ECMWF tends to underestimate maximum daily values of SKT (compared to LST) and slightly overestimate minimum (night-time) temperatures, especially in arid regions such as Northern Africa [48], [50], [80], [81]. Our satellite versus reanalysis comparisons, computed as LST minus SKT (termed LST Delta), exhibit these time-of-day-dependent biases over much of the area and period of study (see Fig. 2).

During summer months, however, coinciding with high concentrations of dust aerosols over the Sahara Desert, the LST Delta signal inverts to being strongly negative. Indeed, LST Delta (for all three LST products) is shown to be related to dust aerosol concentrations (DuAOD), becoming more negative with increased DuAOD. With the use of in situ measurements, we ultimately show that the anomalous LST Delta signal observed during summer months is associated with underestimated satellite LST due to heavy dust aerosol loading.

Given the similar seasonality of water vapor and dust aerosols in the region of study, the relation between LST Delta and atmospheric water vapor content, i.e., TCWV, is also examined. The dependence of LST Delta values on TCWV is shown to be much weaker (see Fig. 4), being slightly more pronounced for MODIS than MSG. Although it is difficult to decouple the effects of water vapor and dust aerosols, there is a stronger relation between the negative LST Delta anomalies and high dust aerosol concentrations, suggesting that this is the primary driver of these anomalies.

In a recent study [88], large biases of the MxD11 LST product were found when compared to ground measurements performed at the Heihe River Basin, an arid region in northwest China. The biases were particularly high during spring, when concentrations of dust aerosols are highest in that region. Although the authors attributed those large errors to the misrepresentation of surface emissivity, it is likely that dust aerosols also play a major role in the inaccuracies. Here, the comparisons against ERA5 over the Sahara region are particularly useful to disentangle the effect of emissivity and aerosols, given that the whole area has fairly stable and similar emissivity values. Since the high LST-SKT differences are mostly confined to the westernmost part of the study region, where DuAOD values are highest, it is possible to pinpoint aerosols as key to the underestimation of satellite LST.

B. Comparison of Satellite LST Against In Situ LST

Recognizing that ERA5's SKT cannot be considered an absolute reference, we use in situ retrievals of LST as an independent reference to both satellites LST and ERA5's SKT. At the two locations analyzed, Niamey and Dahra, the LST products show increased negative biases during the season of high dust aerosol concentrations (i.e., summer) compared to the season of low dust aerosol concentrations (i.e., winter) (see Figs. 5 and 7, Tables I and II). The dispersion and uncertainty of the LST products also generally increased from winter months to summer months, indicating less accurate LST retrievals during the summer. Moreover, the differences between satellite LST and in situ LST (i.e., LST Error) show a clear dependence on DuAOD at the two stations: independent of the time of day and consistent for all three satellite products, LST Error becomes more negative with increased DuAOD [see Figs. 6(a)–(c) and 8(a)–(c)], clearly indicating an underestimation of satellite LST under heavy dust aerosol loading. Although SKT shows a seasonal change in its accuracy when compared to in situ LSTs (see Figs. 5 and 7, Tables I and II), this change in accuracy is not sufficient to account for the negative LST Delta anomalies seen in Fig. 2 and, therefore, cannot be its

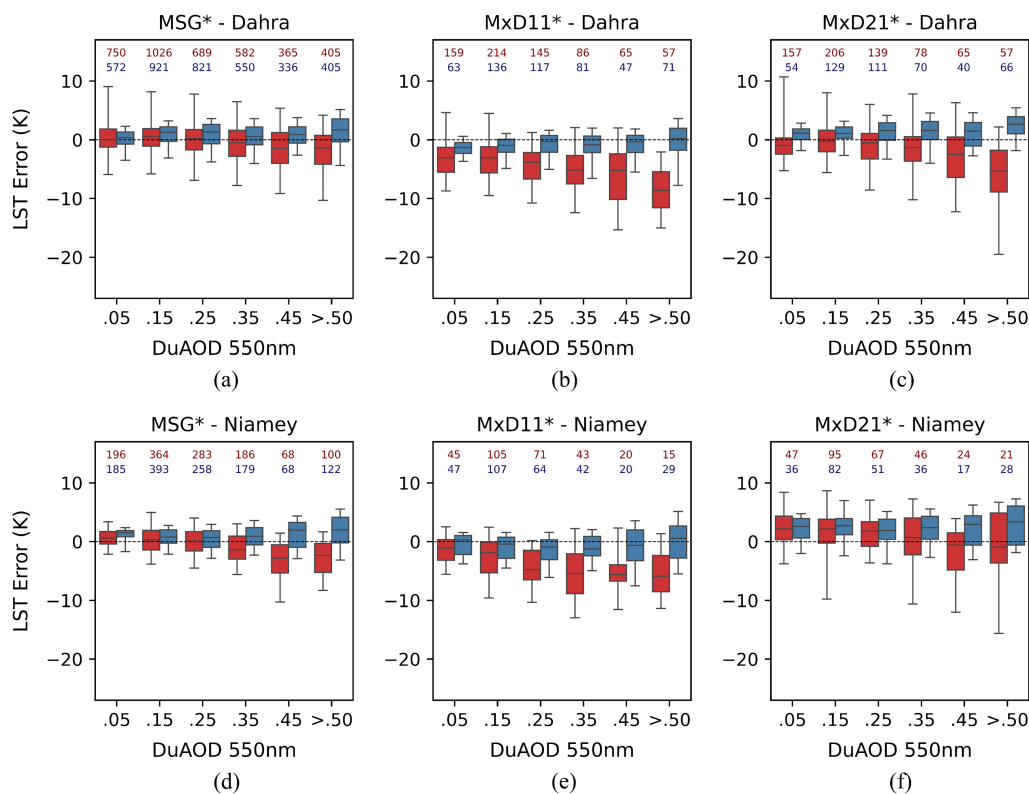


Fig. 10. LST Error as a function of six DuAOD classes using corrected LSTs for Dahra (top panels) and Niamey (bottom panels). The * in the panel titles indicates that the satellite-based LSTs were corrected with the relationship presented in Section IV-D.

primary driver. Furthermore, ERA5's LST Error values are relatively stable with DuAOD [see Figs. 6(d) and 8(d)], suggesting that the changes in LST Delta with DuAOD (Fig. 3) can be mostly attributed to the influence of dust aerosols on the LST products.

The relation between ERA5's LST Error and DuAOD and TCWV [see Figs. 6(d), (h) and 8(d), (h)] suggests that there are various potential sources of error in the SKT estimates. After all, SKT is estimated through a complex surface model that requires a large array of inputs and is limited by the model's representation of surface conditions and their interaction with the atmosphere, making it prone to errors in complex situations such as during episodes of high aerosol concentrations. While a full characterization of these errors exceeds the scope of this study, it is worth noting that ERA5 only uses a monthly climatology of optical depth at the surface [69], [89]. The misrepresentation of peak values in aerosol loading, as well as possible limitations in the simulation of their impact on radiation fluxes, may be a source of SKT errors. It is also relevant to consider that the seasonal pattern of dust aerosols in the Saharan region is closely linked to the ITCZ, which in turn results in similar patterns of atmospheric water vapor concentrations and vegetation density. Vegetation cover may affect SKT due to limitations in the representation of surface emissivity, especially if the representation of vegetation mean values and seasonal dynamics is limited (e.g., [48]). For these reasons, ERA5's SKT is used here only as a means to diagnose the LST products and to assess the extent in space and time of aerosol-induced underestimations.

C. Limitations of Ground Stations

The ground measurements used in this work are essential to unambiguously show the weak performance of the examined LST retrieval algorithms under high dust aerosol concentrations, but they also have limitations, namely 1) the small number of sites offers only a restricted range of atmospheric (dust aerosol and water vapor) and surface conditions; 2) both stations are located in the Sahel region, a transition zone from desert to savanna, meaning the surface around them is not as homogenous as ideally needed to assess the intricate effect of aerosols on LST retrievals. The heterogeneity of the land surface around the station means they have a limited representativeness on the satellite pixel scale. Dahra, for example, is covered by sparse trees and seasonal grass, with a strong greening during the rainy season (July to October) [77], which can introduce discrepancies if not correctly represented in the reanalysis and satellite products. Niamey's measurements, on the other hand, were performed at an airport site [90], which will have highly heterogeneous thermal surface emissions, whereas the surrounding area is mostly urban fabric and sparse vegetation. The full attribution of sources of error at these stations is, therefore, difficult.

D. Evaluation of Aerosol-Induced Underestimation of LST

Assuming that uncertainties in the ground measurements are small compared with the satellite LST Errors, a rough quantitative evaluation of the underestimation under high DuAOD can be made: based on MSG's LST Error in Dahra, by applying a simple

linear regression to the data presented in Fig. 8(a) (daytime and night-time combined), we find an underestimation in satellite LST of approximately 0.9 K for every 0.1 increase in DuAOD. We chose the Dahra station for this evaluation because of its more homogeneous surroundings, and the MSG product because of the larger sample size. The value we obtain is much higher than that simulated by [36] (~ 4 K) and [39] (~ 3 K) for an AOD of 1.0 and a VZA of approximately 25° (MSG's VZA at Dahra). The higher values obtained here may be related to the fact that those studies relied on simulated data, which allows to control each source of error in the LST retrieval, whereas our comparisons against in situ are likely affected by a combination of different error sources. Still, if we apply this correction to the three LST products, the dependence of LST Error (at Dahra and Niamey) on DuAOD significantly decreases (see Fig. 10). Better results are obtained for MSG's LST product since the DuAOD adjustment is based on this product's LST Error, with no accounting of variable viewing angles. It must be stressed that this is only a rough evaluation of the underestimation of LST, devoid of a complete examination of the radiative processes causing it and ignoring aerosol vertical distributions. Even so, until a more comprehensive study of the aerosol effect on LST retrievals is conducted, this correction might be considered by users of LSA SAF's LST product in regions of heavy dust aerosol loading, especially over West Africa in JJA.

E. Analysis of MSG BT Differences

As a brief investigation into the potential causes of the underestimated LSTs, we analyzed MSG's BT differences between the channels centered on 10.8 and 12.0 μm —a key component of MSG's GSW algorithm. In general, for atmospheres with high transmissivity (i.e., dry and transparent), BT differences are mostly controlled by the emissivity difference between the two channels. With the increase of TCWV, the BT difference is known to increase (as shown in Fig. 9). Significantly, dust aerosols have the opposite effect on BT differences compared to water vapor, i.e., higher concentrations lead to more negative BT differences, as indicated by Fig. 9. This response of TIR radiances to the presence of dust aerosols is consistent with findings from other authors [29], [32], [35], [41]. In the studied region, where high DuAOD values occur near or during the wet season (i.e., with moderate-to-high TCWV values), the opposite effects of DuAOD and TCWV on BT differences result in a reduced atmospheric correction performed by the GSW algorithm, as the observed BT difference effectively corresponds to that of a drier atmosphere. This reasoning may explain the relatively high adjustments to DuAOD changes suggested by Dahra's observations (and corroborated by Niamey's data) when compared to previous studies [36], [39].

V. CONCLUSION

In this work, we have shown that LSA SAF's SEVIRI and NASA's MODIS LST products systematically underestimate LST over the Sahara Desert during late spring and summer, when aerosol activity is highest. We find that dust aerosols have the opposite effect on top-of-atmosphere BT differences in the

TIR window compared to water vapor, leading to a reduced atmospheric correction by the LST retrieval algorithms. The underestimation of LST, which in situ measurements suggest may reach up to 9 K for a dust AOD of 1 (at 550 nm), is likely to also occur in other regions with high dust aerosol concentrations, such as the deserts in the Middle East and Central and Southern Asia [46], [47], as well as in the surrounding areas affected by the advection of dust. Furthermore, the fact that such underestimation affects three different LST products, obtained from diverse observations (SEVIRI and MODIS) and algorithm approaches (GSW and TES), means that this issue may also impact other LST products derived from TIR measurements.

The behavior of BT differences observed in conditions of heavy dust aerosol loading is consistent with the wavelength-dependent reduction in atmospheric transmissivity controlled by the dust aerosols' optical properties. However, a layer of dust aerosols not only blocks part of the surface-emitted TIR radiation but also contributes to the atmospheric emission. This is corroborated by preliminary radiative transfer simulations, which indicate that an atmospheric layer with a high concentration of dust aerosols causes a reduction in atmospheric transmissivity and an increase in atmospheric emission, especially in the channel centered at 10.8 μm . These two opposing effects will have to be considered in the development of an aerosol-robust LST retrieval algorithm, which will be the focus of our future work.

ACKNOWLEDGMENT

The authors would like to thank the Atmospheric Radiation Measurement program and the Karlsruhe Institute of Technology for the free access to the in situ data in Niamey (Niger) and Dahra (Senegal), respectively.

REFERENCES

- [1] Z. Su, "The surface energy balance system (SEBS) for estimation of turbulent heat fluxes," *Hydrol. Earth Syst. Sci.*, vol. 6, no. 1, pp. 85–100, 2002.
- [2] X. Zhan and W. P. Kustas, "A coupled model of land surface CO₂ and energy fluxes using remote sensing data," *Agricultural Forest Meteorol.*, vol. 107, no. 2, pp. 131–152, 2001.
- [3] R. D. Crago and R. J. Qualls, "Use of land surface temperature to estimate surface energy fluxes: Contributions of Wilfried Brutsaert and collaborators," *Water Resour. Res.*, vol. 50, no. 4, pp. 3396–3408, 2014.
- [4] J. Sun, G. D. Salvucci, and D. Entekhabi, "Estimates of evapotranspiration from MODIS and AMSR-E land surface temperature and moisture over the Southern Great Plains," *Remote Sens. Environ.*, vol. 127, pp. 44–59, 2012.
- [5] J. D. Kalma, T. R. McVicar, and M. F. McCabe, "Estimating land surface evaporation: A review of methods using remotely sensed surface temperature data," *Surv. Geophys.*, vol. 29, no. 4/5, pp. 421–469, 2008.
- [6] L. Olivera-Guerra, C. Mattar, O. Merlin, C. Durán-Alarcón, A. Santamaría-Artigas, and R. Fuster, "An operational method for the disaggregation of land surface temperature to estimate actual evapotranspiration in the arid region of Chile," *ISPRS J. Photogramm. Remote Sens.*, vol. 128, pp. 170–181, 2017.
- [7] A. J. Arnfield, "Two decades of urban climate research: A review of turbulence, exchanges of energy and water, and the urban heat island," *Int. J. Climatol.*, vol. 23, no. 1, pp. 1–26, 2003.
- [8] J. A. Voogt and T. R. Oke, "Thermal remote sensing of urban climates," *Remote Sens. Environ.*, vol. 86, no. 3, pp. 370–384, 2003.
- [9] M. Bokaie, M. K. Zarkesh, P. D. Arasteh, and A. Hosseini, "Assessment of urban heat island based on the relationship between land surface temperature and land use/land cover in Tehran," *Sustain. Cities Soc.*, vol. 23, pp. 94–104, 2016.

- [10] A. Karnieli et al., "Use of NDVI and land surface temperature for drought assessment: Merits and limitations," *J. Clim.*, vol. 23, no. 3, pp. 618–633, 2010.
- [11] F. N. Kogan, "Operational space technology for global vegetation assessment," *Bull. Amer. Meteorol. Soc.*, vol. 82, no. 9, pp. 1949–1964, 2001.
- [12] D. A. Sims et al., "A new model of gross primary productivity for North American ecosystems based solely on the enhanced vegetation index and land surface temperature from MODIS," *Remote Sens. Environ.*, vol. 112, no. 4, pp. 1633–1646, 2008.
- [13] N. T. Sona, C. F. Chen, C. R. Chen, L. Y. Chang, and V. Q. Minh, "Monitoring agricultural drought in the Lower Mekong Basin using MODIS NDVI and land surface temperature data," *Int. J. Appl. Earth Observ. Geoinf.*, vol. 18, no. 1, pp. 417–427, 2012.
- [14] S. Sruthi and M. A. M. Aslam, "Agricultural drought analysis using the NDVI and land surface temperature data; a case study of Raichur District," *Aquatic Proc.*, vol. 4, pp. 1258–1264, 2015.
- [15] C. Quintano, A. Fernández-Manso, L. Calvo, E. Marcos, and L. Valbuena, "Land surface temperature as potential indicator of burn severity in forest Mediterranean ecosystems," *Int. J. Appl. Earth Observ. Geoinf.*, vol. 36, pp. 1–12, 2015.
- [16] L. Vlassova, F. Pérez-Cabello, M. R. Mimbbrero, R. M. Llovería, and A. García-Martín, "Analysis of the relationship between land surface temperature and wildfire severity in a series of Landsat images," *Remote Sens.*, vol. 6, no. 7, pp. 6136–6162, 2014.
- [17] Z. L. Li et al., "Satellite-derived land surface temperature: Current status and perspectives," *Remote Sens. Environ.*, vol. 131, pp. 14–37, 2013.
- [18] I. F. Trigo, S. L. Ermida, J. P. A. Martins, C. M. Gouveia, F. M. Göttsche, and S. C. Freitas, "Validation and consistency assessment of land surface temperature from geostationary and polar orbit platforms: SEVIRI/MSG and AVHRR/Metop," *ISPRS J. Photogramm. Remote Sens.*, vol. 175, pp. 282–297, 2021.
- [19] P. C. Guillevic et al., "Validation of land surface temperature products derived from the visible infrared imaging radiometer suite (VIIRS) using ground-based and heritage satellite measurements," *Remote Sens. Environ.*, vol. 154, pp. 19–37, 2014.
- [20] N. K. Malakar and G. C. Hulley, "A water vapor scaling model for improved land surface temperature and emissivity separation of MODIS thermal infrared data," *Remote Sens. Environ.*, vol. 182, pp. 252–264, 2016.
- [21] M. A. Martin, D. Ghent, A. C. Pires, F. M. Göttsche, J. Cermak, and J. J. Remedios, "Comprehensive in situ validation of five satellite land surface temperature data sets over multiple stations and years," *Remote Sens.*, vol. 11, no. 5, 2019, Art. no. 479.
- [22] S. B. Duan et al., "Validation of collection 6 MODIS land surface temperature product using in situ measurements," *Remote Sens. Environ.*, vol. 225, pp. 16–29, 2019.
- [23] Z. Wan, "MODIS land-surface temperature algorithm theoretical basis document (LST ATBD)," Inst. Comput. Earth Syst. Sci., Univ. California–Santa Barbara, Santa Barbara, CA, USA, Apr. 1999.
- [24] J. C. Jiménez-Muñoz and J. A. Sobrino, "Error sources on the land surface temperature retrieved from thermal infrared single channel remote sensing data," *Int. J. Remote Sens.*, vol. 27, no. 5, pp. 999–1014, 2006.
- [25] M. Griggs, "A method to correct satellite measurements to sea surface temperature for the effects of atmospheric aerosols," *J. Geophys. Res.*, vol. 90, no. D7, pp. 12951–12959, 1985.
- [26] C. Walton, "Satellite measurement of sea surface temperature in the presence of volcanic aerosols (Hawaii, Gulf-of-Mexico)," *J. Clim. Appl. Meteorol.*, vol. 24, no. 6, pp. 501–507, 1985.
- [27] L. Xu and W. L. Smith, "Numerical simulation of the influence of volcanic aerosols on VAS derived SST determinations," *Appl. Opt.*, vol. 25, no. 7, pp. 1137–1144, 1986.
- [28] S. J. Brown, A. R. Harris, I. M. Mason, and A. M. Závody, "New aerosol robust sea surface temperature algorithms for the along-track scanning radiometer," *J. Geophys. Res., Oceans*, vol. 102, no. C13, pp. 27973–27989, 1997.
- [29] B. Luo, P. J. Minnett, C. Gentemann, and G. Szczodrak, "Improving satellite retrieved night-time infrared sea surface temperatures in aerosol contaminated regions," *Remote Sens. Environ.*, vol. 223, pp. 8–20, 2019.
- [30] D. A. May, L. L. Stowe, J. D. Hawkins, and E. P. McClain, "A correction for Saharan dust effects on satellite sea surface temperature measurements," *J. Geophys. Res., Oceans*, vol. 97, no. C3, pp. 3611–3619, 1992.
- [31] C. J. Merchant, A. R. Harris, M. J. Murray, and A. M. Závody, "Toward the elimination of bias in satellite retrievals of sea surface temperature 1. Theory, modeling and interalgorithm comparison," *J. Geophys. Res., Oceans*, vol. 104, no. C10, pp. 23565–23578, 1999.
- [32] C. J. Merchant, O. Embury, P. L. Borgne, and B. Bellec, "Saharan dust in nighttime thermal imagery: Detection and reduction of related biases in retrieved sea surface temperature," *Remote Sens. Environ.*, vol. 104, no. 1, pp. 15–30, 2006.
- [33] C. J. Merchant and O. Embury, "Adjusting for desert-dust-related biases in a climate data record of sea surface temperature," *Remote Sens.*, vol. 12, no. 16, 2020, Art. no. 2554.
- [34] N. R. Nalli and L. L. Stowe, "Aerosol correction for remotely sensed sea surface temperatures from the National Oceanic and Atmospheric Administration advanced very high resolution radiometer," *J. Geophys. Res., Oceans*, vol. 107, no. C10, pp. 36–1–36–18, 2002.
- [35] X. Quan, H. L. Huang, L. Zhang, E. Weisz, and X. Cao, "Sensitive detection of aerosol effect on simulated IASI spectral radiance," *J. Quant. Spectrosc. Radiat. Transf.*, vol. 122, pp. 214–232, 2013.
- [36] X. Fan et al., "Extension of the generalized split-window algorithm for land surface temperature retrieval to atmospheres with heavy dust aerosol loading," *IEEE J. Sel. Topics Appl. Earth Observ. Remote Sens.*, vol. 8, no. 2, pp. 825–834, Feb. 2015.
- [37] C. Gao et al., "Study of aerosol influence on nighttime land surface temperature retrieval based on two methods," *Adv. Meteorol.*, vol. 2015, 2015, Art. no. 496458.
- [38] X. Fan, G. Nie, H. Wu, and B.-H. Tang, "Estimation of land surface temperature from three thermal infrared channels of MODIS data for dust aerosol skies," *Opt. Express*, vol. 26, no. 4, pp. 4148–4165, 2018.
- [39] E. Zhao, C. Gao, and Y. Yao, "New land surface temperature retrieval algorithm for heavy aerosol loading during nighttime from Gaofen-5 satellite data," *Opt. Express*, vol. 28, no. 2, pp. 2583–2599, 2020.
- [40] A. Labbi, "A study of the impact of aerosols on the estimation of land surface temperature from space using simulation of satellite data," *Turkish J. Remote Sens. GIS*, vol. 2, no. 1, pp. 11–20, 2021.
- [41] L. Bi, S. Ding, R. Zong, and B. Yi, "Examining Asian dust refractive indices for brightness temperature simulations in the 650–1135 cm^{-1} spectral range," *J. Quant. Spectrosc. Radiat. Transf.*, vol. 247, 2020, Art. no. 106945.
- [42] I. F. Trigo et al., "The satellite application facility for land surface analysis," *Int. J. Remote Sens.*, vol. 32, no. 10, pp. 2725–2744, May 2011.
- [43] Z. Wan, "New refinements and validation of the collection-6 MODIS land-surface temperature/emissivity product," *Remote Sens. Environ.*, vol. 140, pp. 36–45, 2014.
- [44] G. C. Hulley, N. K. Malakar, T. Islam, and R. J. Freepartner, "NASA's MODIS and VIIRS land surface temperature and emissivity products: A long-term and consistent earth system data record," *IEEE J. Sel. Topics Appl. Earth Observ. Remote Sens.*, vol. 11, no. 2, pp. 522–535, Feb. 2018.
- [45] I. Tegen, P. Hollrig, M. Chin, I. Fung, D. Jacob, and J. Penner, "Contribution of different aerosol species to the global aerosol extinction optical thickness: Estimates from model results," *J. Geophys. Res., Atmos.*, vol. 102, no. 20, pp. 23895–23915, 1997.
- [46] M. Gavrouzou, N. Hatzianastassiou, A. Gkikas, M. B. Korras-Carraca, and N. Mihalopoulos, "A global climatology of dust aerosols based on satellite data: Spatial, seasonal and inter-annual patterns over the period 2005–2019," *Remote Sens.*, vol. 13, no. 3, 2021, Art. no. 359.
- [47] K. K. Voss and A. T. Evan, "A new satellite-based global climatology of dust aerosol optical depth," *J. Appl. Meteorol. Climatol.*, vol. 59, no. 1, pp. 83–102, 2020.
- [48] F. Johannsen, S. Ermida, J. P. A. Martins, I. F. Trigo, M. Nogueira, and E. Dutra, "Cold bias of ERA5 summertime daily maximum land surface temperature over Iberian Peninsula," *Remote Sens.*, vol. 11, no. 21, 2019, Art. no. 2570.
- [49] M. Nogueira et al., "Upgrading land-cover and vegetation seasonality in the ECMWF coupled system: Verification with FLUXNET sites, METEOSAT satellite land surface temperatures, and ERA5 atmospheric reanalysis," *J. Geophys. Res., Atmos.*, vol. 126, no. 15, 2021, Art. no. e2020JD034163.
- [50] I. F. Trigo, S. Boussetta, P. Viterbo, G. Balsamo, A. Beljaars, and I. Sandu, "Comparison of model land skin temperature with remotely sensed estimates and assessment of surface-atmosphere coupling," *J. Geophys. Res.*, vol. 120, no. 23, pp. 12096–12111, 2015.
- [51] R. Lindstrot et al., "A global climatology of total columnar water vapour from SSM/I and MERIS," *Earth Syst. Sci. Data*, vol. 6, no. 1, pp. 221–233, 2014.

- [52] S. Kinne, "The MACv2 aerosol climatology," *Tellus B, Chem. Phys. Meteorol.*, vol. 71, no. 1, pp. 1–21, 2019.
- [53] I. F. Trigo, I. T. Monteiro, F. Olesen, and E. Kabsch, "An assessment of remotely sensed land surface temperature," *J. Geophys. Res., Atmos.*, vol. 113, no. D17, pp. 1–12, 2008.
- [54] Z. Wan and J. Dozier, "A generalized split-window algorithm for retrieving land-surface temperature from space," *IEEE Trans. Geosci. Remote Sens.*, vol. 34, no. 4, pp. 892–905, Jul. 1996.
- [55] T. R. Loveland et al., "Development of a global land cover characteristics database and IGBP DISCover from 1 km AVHRR data," *Int. J. Remote Sens.*, vol. 21, no. 6/7, pp. 1303–1330, 2000.
- [56] L. F. Peres and C. C. DaCamara, "Emissivity maps to retrieve land-surface temperature from MSG/SEVIRI," *IEEE Trans. Geosci. Remote Sens.*, vol. 43, no. 8, pp. 1834–1844, Aug. 2005.
- [57] I. F. Trigo, L. F. Peres, C. C. DaCamara, and S. C. Freitas, "Thermal land surface emissivity retrieved from SEVIRI/Meteosat," *IEEE Trans. Geosci. Remote Sens.*, vol. 46, no. 2, pp. 307–315, Feb. 2008.
- [58] Z. Wan, S. Hook, and G. Hulley, "MODIS/Aqua land surface temperature/emissivity daily L3 global 0.05Deg CMG V061," *NASA EOSDIS Land Process. DAAC*, 2021, doi: [10.5067/MODIS/MYD11C1.061](https://doi.org/10.5067/MODIS/MYD11C1.061).
- [59] Z. Wan, S. Hook, and G. Hulley, "MODIS/Terra land surface temperature/emissivity daily L3 global 0.05Deg CMG V061," *NASA EOSDIS Land Process. DAAC*, 2021, doi: [10.5067/MODIS/MOD11C1.061](https://doi.org/10.5067/MODIS/MOD11C1.061).
- [60] Z. Wan, S. Hook, and G. Hulley, "MODIS/Aqua land surface temperature/emissivity daily L3 global 1km SIN Grid V061," *NASA EOSDIS Land Process. DAAC*, 2021, doi: [10.5067/MODIS/MYD11A1.061](https://doi.org/10.5067/MODIS/MYD11A1.061).
- [61] Z. Wan, S. Hook, and G. Hulley, "MODIS/Terra land surface temperature/emissivity daily L3 global 1km SIN Grid V061," *NASA EOSDIS Land Process. DAAC*, 2021, doi: [10.5067/MODIS/MOD11A1.061](https://doi.org/10.5067/MODIS/MOD11A1.061).
- [62] G. Hulley and S. Hook, "MODIS/Aqua land surface temperature/3-band emissivity daily L3 global 0.05Deg CMG V061," *NASA EOSDIS Land Process. DAAC*, 2021, doi: [10.5067/MODIS/MYD21C1.061](https://doi.org/10.5067/MODIS/MYD21C1.061).
- [63] G. Hulley and S. Hook, "MODIS/Terra land surface temperature/3-band emissivity daily L3 global 0.05Deg CMG V061," *NASA EOSDIS Land Process. DAAC*, 2021, doi: [10.5067/MODIS/MOD21C1.061](https://doi.org/10.5067/MODIS/MOD21C1.061).
- [64] G. Hulley, "MODIS/Aqua land surface temperature/3-band emissivity daily 13 global 1km SIN grid day V061," *NASA EOSDIS Land Process. DAAC*, 2021, doi: [10.5067/MODIS/MYD21A1D.061](https://doi.org/10.5067/MODIS/MYD21A1D.061).
- [65] G. Hulley and S. Hook, "MODIS/Aqua land surface temperature/3-band emissivity daily L3 global 1km SIN Grid Night V061," *NASA EOSDIS Land Process. DAAC*, 2021, doi: [10.5067/MODIS/MYD21A1N.061](https://doi.org/10.5067/MODIS/MYD21A1N.061).
- [66] G. Hulley and S. Hook, "MODIS/Terra land surface temperature/3-band emissivity daily L3 global 1km SIN Grid Day V061," *NASA EOSDIS Land Process. DAAC*, 2021, doi: [10.5067/MODIS/MOD21A1D.061](https://doi.org/10.5067/MODIS/MOD21A1D.061).
- [67] G. Hulley and S. Hook, "MODIS/Terra land surface temperature/3-band emissivity daily L3 global 1km SIN Grid Night V061," *NASA EOSDIS Land Process. DAAC*, 2021, doi: [10.5067/MODIS/MOD21A1N.061](https://doi.org/10.5067/MODIS/MOD21A1N.061).
- [68] A. Gillespie, S. Rokugawa, T. Matsunaga, J. S. Cothorn, S. Hook, and A. B. Kahle, "A temperature and emissivity separation algorithm for advanced spaceborne thermal emission and reflection radiometer (ASTER) images," *IEEE Trans. Geosci. Remote Sens.*, vol. 36, no. 4, pp. 1113–1126, Jul. 1998.
- [69] H. Hersbach et al., "The ERA5 global reanalysis," *Quart. J. Roy. Meteorol. Soc.*, vol. 146, no. 730, pp. 1999–2049, 2020.
- [70] A. Inness et al., "The CAMS reanalysis of atmospheric composition," *Atmos. Chem. Phys.*, vol. 19, no. 6, pp. 3515–3556, 2019.
- [71] M. Thomas, C. Gautier, and P. Ricchiuzzi, "Investigations of the March 2006 African dust storm using ground-based column-integrated high spectral resolution infrared (8–13 μm) and visible aerosol optical thickness measurements: 1. Measurement procedures and results," *J. Geophys. Res., Atmos.*, vol. 114, no. D11, pp. 1–12, 2009.
- [72] C. Pierangelo, A. Chédin, S. Heilliette, N. Jacquinet-Husson, and R. Armante, "Dust altitude and infrared optical depth from AIRS," *Atmos. Chem. Phys.*, vol. 4, no. 7, pp. 1813–1822, 2004.
- [73] S. G. DeSouza-Machado, L. L. Strow, S. E. Hannon, and H. E. Motteler, "Infrared dust spectral signatures from AIRS," *Geophys. Res. Lett.*, vol. 33, no. 3, pp. 1–5, 2006.
- [74] M. Sengupta and M. Kutchenreiter, "Radiation measurements at AMF (RAD). Atmospheric radiation measurement (ARM) user facility," 2006, doi: [10.5439/1190146](https://doi.org/10.5439/1190146).
- [75] P. Guillevic et al., "Land surface temperature product validation best practice protocol version 1.1," Best Practice for Satellite-Derived Land Product Validation: Land Product Validation Subgroup (WGCV/CEOS), 2018.
- [76] N. JPL, "ASTER global emissivity dataset, 100-meter, HDF5," *NASA EOSDIS Land Process. DAAC*, 2014, doi: [10.5067/Community/ASTER_GED/AG100.003](https://doi.org/10.5067/Community/ASTER_GED/AG100.003).
- [77] F. M. Göttsche, F. S. Olesen, I. F. Trigo, A. Bork-Unkelbach, and M. A. Martin, "Long term validation of land surface temperature retrieved from MSG/SEVIRI with continuous in-situ measurements in Africa," *Remote Sens.*, vol. 8, no. 5, 2016, Art. no. 410.
- [78] D. E. Waliser and C. Gautier, "A satellite-derived climatology of the ITCZ," *J. Clim.*, vol. 6, no. 11, pp. 2162–2174, 1993.
- [79] N. Žagar, G. Skok, and J. Tribbia, "Climatology of the ITCZ derived from ERA Interim reanalyses," *J. Geophys. Res., Atmos.*, vol. 116, no. 15, pp. 1–6, 2011.
- [80] A. Wang, M. Barlage, X. Zeng, and C. S. Draper, "Comparison of land skin temperature from a land model, remote sensing, and in situ measurement," *J. Geophys. Res., Atmos.*, vol. 119, no. 6, pp. 3093–3106, 2014.
- [81] W. Zheng et al., "Improvement of daytime land surface skin temperature over arid regions in the NCEP GFS model and its impact on satellite data assimilation," *J. Geophys. Res., Atmos.*, vol. 117, no. D6, pp. 1–14, 2012.
- [82] F. E. Volz, "Infrared optical constants of ammonium sulfate, Sahara dust, volcanic pumice, and flyash," *Appl. Opt.*, vol. 12, no. 3, pp. 564–568, 1973.
- [83] F. E. Volz, "Infrared refractive index of atmospheric aerosol substances," *Appl. Opt.*, vol. 11, no. 4, pp. 755–759, 1972.
- [84] S. C. Freitas, I. F. Trigo, J. Macedo, C. Barroso, R. Silva, and R. Perdigão, "Land surface temperature from multiple geostationary satellites," *Int. J. Remote Sens.*, vol. 34, no. 9/10, pp. 3051–3068, 2013.
- [85] Y. Yu et al., "Developing algorithm for operational GOES-R land surface temperature product," *IEEE Trans. Geosci. Remote Sens.*, vol. 47, no. 3, pp. 936–951, Mar. 2009.
- [86] Y. Liu, Y. Yu, P. Yu, H. Wang, and Y. Rao, "Enterprise LST algorithm development and its evaluation with NOAA 20 data," *Remote Sens.*, vol. 11, no. 17, 2019, Art. no. 2003.
- [87] D. J. Ghent, G. K. Corlett, F. M. Göttsche, and J. J. Remedios, "Global land surface temperature from the along-track scanning radiometers," *J. Geophys. Res., Atmos.*, vol. 122, no. 22, pp. 12167–12193, 2017.
- [88] L. Lu, T. Zhang, T. Wang, and X. Zhou, "Evaluation of collection-6 MODIS land surface temperature product using multi-year ground measurements in an arid area of northwest China," *Remote Sens.*, vol. 10, no. 11, 2018, Art. no. 1852.
- [89] H. Hersbach, C. Peubey, A. Simmons, P. Berrisford, P. Poli, and D. Dee, "ERA-20CM: A twentieth-century atmospheric model ensemble," *Quart. J. Roy. Meteorol. Soc.*, vol. 141, no. 691, pp. 2350–2375, 2015.
- [90] A. Slingo et al., "Overview of observations from the RADAGAST experiment in Niamey, Niger: Meteorology and thermodynamic variables," *J. Geophys. Res., Atmos.*, vol. 114, no. 13, 2009, Art. no. D00E01.



Francesco Stante was born in Lisbon, Portugal, in 1997. He received the B.S. degree in meteorology, oceanography, and geophysics from the University of Lisbon, Lisbon, Portugal, in 2021. He is currently working toward the M.Sc. degree in geophysical sciences with the University of Lisbon, Lisbon, Portugal. He is also with the Portuguese Institute for Sea and Atmosphere within the framework of the LSA SAF Project.



Sofia L. Ermida was born in Lisbon, Portugal, in 1990. She received the B.S. degree in meteorology, oceanography, and geophysics, the M.Sc. degree in geophysical sciences, and the Ph.D. degree in geophysical sciences and geoinformation with specialization in remote sensing from the University of Lisbon, Lisbon, Portugal, in 2011, 2013, and 2018, respectively.

She is currently an Associate Researcher with the Portuguese Institute for Sea and Atmosphere, Lisbon, Portugal. Her current research focuses on land surface temperature estimation from remote sensors.



Carlos C. DaCamara received the Ph.D. degree in atmospheric science from the University of Missouri, Columbia, MO, USA, in 1991.

He is currently an Associate Professor with the Faculty of Sciences, University of Lisbon, Lisbon, Portugal, and is a Senior Researcher with the Instituto Dom Luiz, University of Lisbon. His research interests include the use of satellite information for surface temperature and emissivity retrieval, burned area mapping and vegetation recovery assessment after large wildfires, the development and calibration of indices of meteorological fire danger, the characterization of the atmospheric circulation associated to extreme weather events (such as droughts and heat-waves), and the study of planetary wave activity and its implications on climate variability.



Isabel F. Trigo received the B.S. and M.Sc. degrees in geophysical sciences from the University of Lisbon, Lisbon, Portugal, in 1993 and 1997, respectively, and the Ph.D. degree in climatology from the University of East Anglia, Norwich, U.K., in 2000.

In 2001, after a period working with the European Centre for Medium-Range Weather Forecasts as a Visiting Scientist, she joined the Portuguese Meteorology Institute (now IPMA), Lisbon, Portugal, where she has been working on remote sensing applications to derive land surface variables, and on their use to better understand and model land surface processes. She leads IPMA's Earth Observation Unit, which hosts the EUMETSAT Satellite Applications Facility on Land Surface Analysis.



Frank-Michael Götsche received the M.Sc. degree in physics and the Ph.D. degree in geophysics from the University of Kiel, Kiel, Germany, in 1993 and 1997, respectively.

From 1996 to 1997, he was a Research Scholar with the Department of Earth Sciences, Uppsala University, Uppsala, Sweden. From 1997 to 2003, he was a Research Scientist with the Institute of Meteorology and Climate Research, Forschungszentrum Karlsruhe, Karlsruhe, Germany. He then became an Assistant Professor with United Arab Emirates University, Al Ain, UAE, where he lectured physics and remote sensing classes and was a Scientific Consultant to EUMETSAT's Land Surface Analysis Satellite Application Facility. Since 2007, he has been a Senior Researcher with Karlsruhe Institute of Technology (KIT), Karlsruhe, where he leads the validation efforts of several EUMETSAT and European Space Agency projects for satellite retrieved surface temperature products. Building on KIT's in situ radiance measurements dedicated to land surface temperature validation, he is also actively involved in the development of reconstruction and spatiotemporal fusion techniques.